Measurement of the Absolute Temporal Coupling between DNA Binding and Base Flipping†

Barrett W. Allan,‡,§ Norbert O. Reich,*,‡ and Joseph M. Beechem*,||

Department of Chemistry and Program in Biochemistry and Molecular Biology, University of California, Santa Barbara, California 93106-6081, and Department of Molecular Physiology and Biophysics, Vanderbilt University Medical Center, Nashville, Tennessee 37232-0615

Received January 4, 1999; Revised Manuscript Received March 3, 1999

ABSTRACT: The absolute temporal couplings between DNA binding and base flipping were examined for the *Eco*RI DNA methyltransferase. The binding event (monitored using rhodamine-x fluorescence anisotropy) was monophasic with a second-order on-rate of 1.1×10^7 M^{-1} $s^{-1} \leq k_{on} \leq 2.25 \times 10^7$ M^{-1} s^{-1}. Base-flipping kinetics (monitored using 2-aminopurine fluorescence intensity) were essentially synchronous with the binding kinetics, with less than a 4 ms delay between enzyme binding and target base flipping. The 4 ms delay translates into a base-flipping rate of at least 195 s^{-1}, when the data are analyzed in terms of a sequential DNA binding and base-flipping reaction mechanism. Synchrony of binding and base flipping was only observed during the first 80% of the reaction, and an additional 20% base-flipping signal occurred well after DNA binding was complete. This additional 2AP fluorescence change, with an effective rate of 0.55 s^{-1}, is an intramolecular isomerization reaction which greatly accelerates the dissociation of the enzyme from DNA. The correlation between the dissociation of the enzyme−DNA complex and the restacking of the extrahelical base also revealed a very tight coupling of these two events. Both dissociation and base restacking were found to be biphasic. These data are consistent with the following mechanism. The initial binding rate and base-flipping rates map very closely with previously determined pre-steady-state burst-rate kinetics for methyl transfer. Hence, binding, flipping, and methylation appear to occur in nearly a single concerted step. The bound complex then slowly isomerizes (0.1 s^{-1}) to a distinct configuration that accelerates the product-release phase of the reaction. The product-release enzyme configuration dissociates from DNA approximately 8 times faster than the initial bound complex (0.18 s^{-1} vs 0.024 s^{-1}). When the enzyme dissociates from the DNA along the product-release pathway, the target base remains in an extrahelical conformation and restacks at a rate of only 0.6 s^{-1}. This "multicolor" fluorescence kinetic approach directly measures the absolute temporal correlation between DNA binding and base flipping, with millisecond timing resolution. The data reveal that even when the B-DNA structure is altered in a radical manner (e.g., via base flipping), enzymes can perform this operation in a highly efficient, if not completely concerted manner.

Enzyme−DNA interactions often demand significant distortion of the DNA away from a B-form conformation to permit catalysis. Determination of the temporal correlation between the binding of the enzyme to the DNA and the subsequent alteration in DNA conformation provides a means to understand the mechanistic importance of the enzyme-induced changes in DNA structure. A striking example of such a catalytically essential distortion of the DNA away from a B-form is the rotation of a nucleotide 180° out of the DNA double helix and into an enzyme active site cavity (i.e., "base flipping"). Structural data (*1*−*4*), functional data (*5*−*7*), and sequence comparisons (*8*) strongly imply that all DNA methyltransferases invoke base flipping prior to methyl group transfer. Several classes of DNA repair enzymes also stabilize an extrahelical base during the catalytic cycle (*9*, *10*). The collective studies show for DNA-modifying enzymes that the stabilization of an extrahelical base is central to catalysis and can provide a mechanism of establishing specificity.

2-Aminopurine (2AP)[1] is a very sensitive spectroscopic marker for base flipping at the target site by M.*Eco*RI (*5*, *7*). This work and earlier studies using more classical

† The work was supported by NSF Grant MCB-9603567 to N.O.R. and NIH Grants GM45990 and GM58588 to J.M.B.

* Correspondence can be addressed to either author. N.O.R.: telephone (805) 893-8368, fax (805) 893-4120, e-mail reich@chem.ucsb.edu. J.M.B.: telephone (615) 322-7980, fax (615) 322-7236, e-mail joe.beechem@mcmail.vanderbilt.edu.

‡ University of California, Santa Barbara.

§ Current address: Maxygen, Inc., 3410 Central Expressway, Santa Clara, CA 95051.

|| Vanderbilt University Medical Center.

[1] Without a cocrystal structure of *Eco*RI DNA N^6 adenine methyltransferase on a 2-aminopurine-containing oligonucleotide, it is not possible to unequivocally state that the fluorescence change observed represents base flipping. The measured fluorescence enhancement, however, is unique to the target site and clearly monitors altered base-stacking properties induced at the target site (*5*, *7*; for 2AP studies with a base-flipped cocrystal structure see, e.g., ref *31*). Detailed control experiments which directly address the uniqueness of the 2AP signal for the target site base can be found in refs *5* and *7*. The following abbreviations are used: M.*Eco*RI, *Eco*RI DNA N^6 adenine methyltransferase; 2AP, 2-aminopurine; RHX, rhodamine-x 5- (and 6-) isothiocyanate. The target base within a specific recognition site (of listed DNA sequences) is underlined.

10.1021/bi9900020 CCC: $18.00
Published on Web 04/06/1999

biochemical approaches show that the methylation of the target base by M.*Eco*RI must occur extremely rapidly after base flipping (*7*, *11*). We further extend this work herein using a "two-color" spectroscopic assay that enables the simultaneous (and independent) observation of both DNA binding and base flipping. Binding is detected by changes in the fluorescence anisotropy of rhodamine-x tethered to the 5′-end of the DNA (red fluorescence signal), and altered base stacking is observed by changes in the fluorescence intensity of 2AP incorporated at the target base (blue fluorescence signal). The distinct fluorescence signatures and sensitivities of these probes enable the absolute temporal correlation between the DNA binding event and the disruption of base stacking to be determined, thereby providing direct insight into the kinetic mechanism of sequence-specific DNA base recognition and flipping.

MATERIALS AND METHODS

Enzyme Expression and Purification. M.*Eco*RI was overexpressed from pXRI and purified to apparent homogeneity as described (*12*). M.*Eco*RI concentration (108 μM) was determined spectrophotometrically utilizing the reported extinction coefficient ($E_{280}^{1mM} = 10.8$) (*13*). The specific activity of the enzyme preparation was determined using pre-steady-state burst-magnitude determinations in the presence of [^{3}H]-*S*-adenosyl-L-methionine as described (*14*) and shown to be fully active.

Oligonucleotide Synthesis and Purification. All oligonucleotides (14-mers) utilized in these studies were synthesized on a Cyclone 8400 Plus DNA synthesizer (Milligen/Biosearch, Burlington, MA) using β-cyanoethyl phosphoramidites with the final dimethoxytrityl group present. 2-Aminopurine phosphoramidite was purchased from Glenn Research (Sterling, VA), standard and N^6-methyladenosine phosphoramidites were from Pharmacia Biotech Inc., and rhodamine-x 5- (and 6-) isothiocyanate (X-491) was from Molecular Probes (Eugene, OR). Oligonucleotides were purified by HPLC using a Dynamax C18 reversed-phase PureDNA column (Rainin Instrument Co.). For the extrinsic labeling of the DNA with RHX, oligonucleotides were synthesized that contained a primary amino group connected by a six methylene spacer to the 5′-end (5′ Amino Modifier C6, Glenn Research). These 5′-modified oligonucleotides eluted from the C18 column approximately 5 min later than DNA lacking modification (data not shown). For standard oligonucleotides, DNA purity was assessed by radiolabeling with T4 polynucleotide kinase (New England Biolabs) and [γ-^{32}P]ATP, 20% denaturing polyacrylamide gel electrophoresis, and visualization by autoradiography. The 5′-modified DNA was inefficiently radiolabeled, and purity was assessed by ethidium bromide staining. Extrinsic labeling of the DNA with the RHX fluorophore was performed essentially as described (*15*). Briefly, the 5′-modified DNA was precipitated in ethanol, and following centrifugation the DNA pellet was resuspended in a 0.1 M sodium carbonate/sodium bicarbonate buffer (pH 9.0) at a concentration of 0.5 mM. RHX isothiocyanate was dissolved in *N*,*N*-dimethylformamide (Fisher Scientific) at a concentration of 10 mg/mL and added dropwise to the oligonucleotide solution (9-fold final molar probe excess), and the reaction was stirred overnight in the dark at 25 °C. Following incubation, solutions were mixed with denaturing gel loading buffer, heated briefly, and loaded onto a prerunning 12% polyacrylamide gel followed by electrophoresis for 3−5 h at 400 V. The unreacted probe was efficiently separated from the RHX-coupled DNA product because it did not significantly migrate into the gel. In contrast, the RHX-coupled DNA migrated as a visible band of "fluorescent DNA". This DNA was eluted from gel slices at 55 °C into a pH 7.0 buffer containing 0.1 M (triethylamino)ammonium acetate, supplemented with 0.1 mM EDTA. The eluted DNA was dried using a Speedvac concentrator and resuspended in TE buffer (10 mM Tris, 1 mM EDTA, pH 8.0). DNA concentrations were determined spectrophotometrically at 260 nm with an extinction coefficient calculated using software based upon the reported pairwise base extinction data (*16*). The following 14 base pair DNA oligonucleotides were annealed at an equimolar ratio in H_2O with 100 mM NaCl utilizing an MJ Research (Watertown, MA) programmable thermocycler: d(RHXGGCGGAATTCGCGG) and d(CCGCGAXTTCCGCC), where RHX = rhodamine-x X = adenine or 2-aminopurine. Native polyacrylamide gel electrophoresis of the doubly labeled DNA could not detect the presence of any single-stranded component.

Steady-State Fluorescence Measurements. Steady-state fluorescence emission spectra were collected from 340 to 700 nm on a SPEX 1681 Fluorolog spectrophotometer (Edison, NJ) by exciting the sample at 310 nm. The excitation and emission bandwidths were 5 nm for all the spectra. Solutions contained 200 nM DNA and were titrated with increasing concentration of M.*Eco*RI.

Stopped-Flow System and Photon Counting Fluorescence Detection. An SFM-3 stopped-flow unit containing three independently driven stepper-motor syringes (Molecular Kinetics, Pullman, WA) with a 50 μL cuvette and a hard-stop shutter was used. Fluorescence detection for the stopped-flow studies utilized a two-channel single-photon detector unit consisting of the following: a Hamamatsu R928 photomultiplier, a 5 × 300 MHz amplifier (Stanford Research SR445, Sunnyvale, CA), a discriminator (Stanford Research SR400), and two multichannel scaler cards (Tennelec Model MCS-II, Oak Ridge, TN), interfaced to two microcomputers (Intel 486). A 450 W xenon arc lamp (SPEX Fluorolog Model 1681) with fiber-optic output was directed into the 50 μL observation cuvette. The detection system was activated by an external synch-out pulse from a Molecular Kinetics stepper-motor controlling unit. Data acquisition began at least 100 ms before sample mixing and were collected in 8000 total channels with varied dwell time depending upon the experiment. For 2AP total intensity experiments, excitation was at 310 nm and the fluorescence emission from detection channel 1 was spectrally isolated from the RHX signal using a 340 nm cutoff filter (Hoya Optics, Freemont, CA) in combination with a blue "notch filter" (Oriel, Stratford, CT). For RHX anisotropy binding experiments, a T-format anisotropy detection scheme was used; $\lambda_{ex} = 580$ nm, and λ_{em} was collected through a 620 nm cutoff filter. For two-color experiments, the data from five 2AP total intensity time courses were summed, followed by five RHX anisotropy time courses. Polarizers were placed at the end of the fiber-optic excitation source, and the λ_{ex} was toggled between 310 and 580 during the alternating data collection modes. This process was repeated until an adequate signal-to-noise ratio was achieved. All stopped-flow experi-

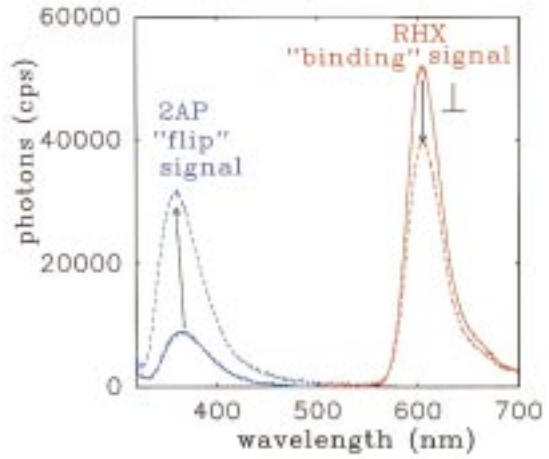

FIGURE 1: Steady-state fluorescence emission spectrum of the two-color DNA unliganded in solution (solid line) and bound by saturating M.*Eco*RI (broken line). Blue spectral region: 2-aminopurine "flip" signal, $\lambda_{ex} = 310$ nm and $\lambda_{em} = 360$ nm. The large increase in fluorescence intensity and 10 nm blue-shift in the emission λ_{max} occur following enzyme binding due to loss of intrastrand base-stacking interactions. Red spectral region: rhodamine-x "binding" signal, $\lambda_{ex} = 580$ nm, $\lambda_{em} = 620$ nm cut-on filter, and T-format detection scheme. Horizontal polarization decreases upon M.*Eco*RI binding. A solution containing 200 nM two-color DNA, 100 μM sinefungin, 100 mM Tris, 10 mM EDTA, 100 mM NaCl, and 1 mM DTT at pH 7.5 was titrated with increasing M.*Eco*RI.

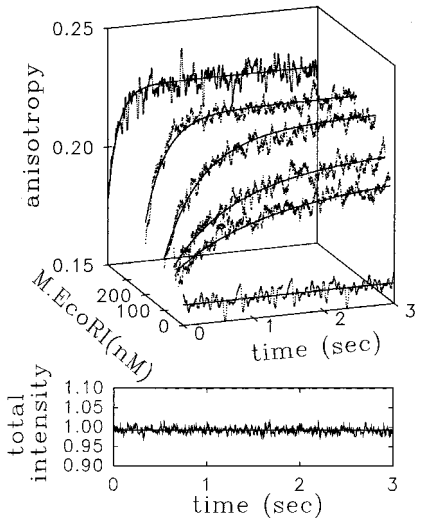

FIGURE 2: Determination of the second-order binding rate constant. At $t = 0$, 20 nM DNA was rapidly mixed with 0, 25, 50, 100, 200, or 400 nM enzyme (final concentration) in the same buffer described in Figure 1. For clarity, only every third data point is shown. Smooth lines through the data represent the global analysis of the stopped-flow data using a single second-order on-rate. Rigorous error analysis yields (at the 95%) confidence level 1.1×10^7 M^{-1} s^{-1} $\leq k_{on} \leq 2.25 \times 10^7$ M^{-1} s^{-1}. The lower panel shows that the RHX fluorescence total intensity is unaffected by M.*Eco*RI binding, confirming that the anisotropy signal changes (upper panel) are due entirely to differences in fluorescence anisotropy.

ments contained less than 2.0% glycerol. Solutions of enzyme (diluted into a degassed buffer containing 200 μM sinefungin, 100 mM Tris, 10 mM EDTA, 100 mM NaCl, and 1 mM DTT at pH 7.5), double-stranded duplex DNA, and buffer alone each were loaded into separate syringes. Reactions (200 μL) were initiated by mixing equal volumes (100 μL) of enzyme and DNA solutions at flow rates between 4 and 10 mL s^{-1}. Background subtractions for the on-rate experiments were made using the measured 2AP intensity and RHX anisotropy signals of the DNA duplex and buffer alone prior to mixing the enzyme and DNA solutions. For the off-rate experiments background controls included the prebound ternary complex (enzyme−DNA−sinefungin) and 14 base pair duplex DNA lacking either modification.

RESULTS AND DISCUSSION

Steady-State 2AP Fluorescence Total Intensity and RHX Fluorescence Anisotropy. The corrected steady-state fluorescence emission spectrum of the two-color DNA alone (solid line) and the spectrum following titration with saturating M.*Eco*RI (broken line) are shown in Figure 1. The large separation between the base-flipping signal (λ_{max} 360 nm) and the DNA binding signal (λ_{max} 603 nm) enables the spectroscopic observation of both processes with absolutely no interference (i.e., no cross-talk between detection channels). Nucleosides and nucleotides containing the 2AP base are highly fluorescent in solution but strongly quenched (>95%) upon incorporation into duplex DNA (*7*, *17*, *18*). The relatively long excitation λ_{max} (~310 nm) of the 2AP probe enables its selective excitation in the presence of protein. These fluorescence properties make 2AP an excellent and widely applicable probe for the disruption of nearest-neighbor base stacking caused by enzyme−DNA interactions. The binding of M.*Eco*RI to duplex DNA substituted with 2AP at the target base within the *Eco*RI recognition site (5′-GAATTC-3′) produces a large steady-state fluorescence intensity increase and a 10 nm blue shift in the emission λ_{max} (*5*, *7*) (Figure 1).

The covalent labeling of DNA with dyes such as fluorescein or rhodamine-x can be used to monitor complex formation in solution under steady-state (*19*, *20*) and pre-steady-state conditions (*15*, *21*, *22*). DNA binding is detected by changes in the anisotropy (or polarization) of the extrinsic fluorophore. DNA bound by a protein has slower Brownian tumbling motion relative to unliganded DNA. The slower global tumbling motion of the complex is detected as an increase in the steady-state anisotropy value. Figure 1 shows that, using a vertically polarized excitation source, the horizontal polarization of the RHX binding probe decreases following the assembly of M.*Eco*RI onto the two-color DNA. The corresponding vertically polarized component increases (data not shown), resulting in a large change in the fluorescence anisotropy. Time-resolved fluorescence lifetime measurements of the free and bound states are completely superimposable, showing that the RHX signal changes are not due to lifetime differences (data not shown; see total intensity control in Figure 2). Use of this multiprobe strategy in a pre-steady-state assay enables direct real-time observation of enzyme−DNA interaction with high signal-to-noise and millisecond timing resolution.

Determination of the Second-Order Binding Rate Constant. To confirm that the rhodamine-x anisotropy signal change was a direct monitor of M.*Eco*RI binding, the second-order binding rate constant (k_{on}) was determined. Real-time association kinetics were examined as a function of enzyme concentration. Stopped-flow anisotropy data obtained with 20 nM RHX-labeled DNA and 0, 25, 50, 100, 200, and 400 nM M.*Eco*RI are shown in Figure 2. Global nonlinear analysis of the on-rate data followed by rigorous error

analysis (*23*) revealed that at the 95% confidence level $1.1 \times 10^7\ M^{-1}\ s^{-1} \leq k_{on} \leq 2.25 \times 10^7\ M^{-1}\ s^{-1}$.

The second-order association rate constant recovered from the global analysis of the stopped-flow data is reasonably consistent with an indirect k_{on} ($4.2 \times 10^7\ M^{-1}\ s^{-1}$) calculated from k_{off} and K_D^{DNA} determinations made from gel mobility shift assays with a 14 base pair DNA duplex (*24*). The k_{cat}/K_m^{DNA} ($2.4 \times 10^7\ M^{-1}\ s^{-1}$) determined with an identically sized DNA substrate is even closer in agreement with the on-rate (*25*). The clear M.*Eco*RI concentration-dependent increase in anisotropy signal (Figure 2) can be rigorously analyzed in terms of a second-order binding process, supporting the use of RHX-labeled DNA to quantify the real-time binding interactions of M.*Eco*RI with target sequence DNA. The internal consistency of the RHX anisotropy determined on-rate with previous (albeit) indirect approaches further strengthens this assignment. The lower panel in Figure 2 shows that the RHX total intensity is insensitive to M.*Eco*RI binding and that the signal changes within the bound complex are due entirely to differences in RHX fluorescence anisotropy, consistent with the lifetime measurements.

Although these experiments were done at saturating concentrations of the cofactor analogue sinefungin (*28*), binary (enzyme−DNA) complex formation occurs approximately 100-fold slower than ternary (enzyme−DNA−sinefungin) complex formation. A strongly cofactor-dependent equilibrium between distinct enzyme forms exists for M.*Eco*RI, and a hyperbolic dependence of the effective on-rate is observed with respect to cofactor concentration (B. W. Allan, J. M. Beechem, and N. O. Reich, manuscript in preparation).

Two-Color Observation of DNA Binding and Base Unstacking. Having established that the anisotropy signal changes in the RHX-labeled DNA enable a direct measure of DNA binding by M.*Eco*RI, two-color DNA duplexes were synthesized. In two-color DNA, 2AP is site-specifically incorporated at the target base in addition to the RHX binding probe at the 5′-end of the DNA. Incorporating the different probes into the same DNA duplex enables direct and simultaneous spectroscopic observation of DNA binding and base flipping (see Figure 1 for steady-state end points). While one could (in theory) perform sequential stopped-flow studies on individual singly labeled DNAs, we found that small alterations in the binding/dissociation rates of the singly labeled species (a maximum change of ∼10%−35%) made direct and absolute comparison much more problematic. Stopped-flow measurements on the doubly labeled DNA allows a direct and absolute comparison of signals to be performed without the need for "labeling-correction" terms to be applied to the data. The relative affinities of the enzyme for doubly labeled and nonlabeled DNA were very similar (±25%; data not shown).

Combined 2AP fluorescence intensity and RHX fluorescence anisotropy pre-steady-state kinetic data obtained at 200 nM two-color DNA and 400 nM M.*Eco*RI are shown in Figure 3. Under these reaction conditions, the DNA binding and base-flipping signals nearly superimpose during the first 400 ms of the reaction (Figure 3 inset). Analysis of both data sets in terms of exponential signal increases yields a dominant (∼80%) term of 17.6 s^{-1} in the 2AP data, nearly identical to the monophasic RHX anisotropy binding data

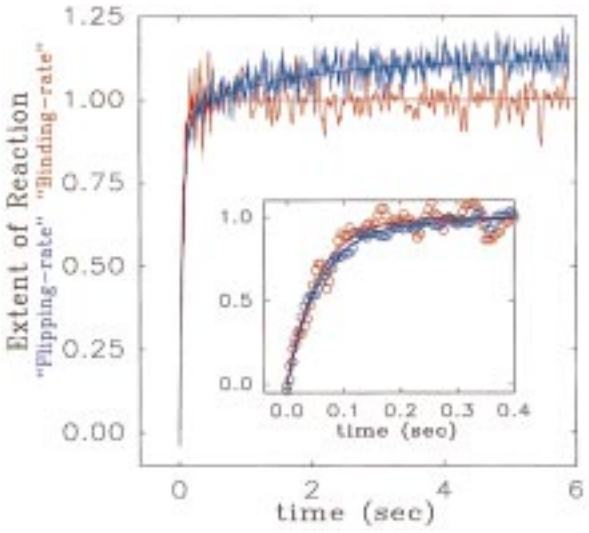

FIGURE 3: Determination of the absolute temporal coupling between the "binding rate" (red fluorescence signal) and target base "flipping rate" (blue fluorescence signal) for the M.*Eco*RI interaction with two-color duplex DNA. The data were collected following the rapid mixing of 200 nM two-color DNA and 400 nM enzyme in the stopped-flow system. The smooth lines represent the nonlinear least-squares fit to the data. The RHX binding signal change was best described by a single-exponential analysis yielding a rate constant of 18.4 s^{-1}, with the 2AP flipping data best described by the sum of two exponentials (t in seconds): $0.85 \exp(17.6t) + 0.15 \exp(0.5t)$. The inset shows data collected during the first 400 ms of the experiment. The rate constants obtained from nonempirical analysis of these data directly in terms of the coupling between second-order binding and base flipping are shown in Scheme 1 and described in the text.

(18.4 s^{-1}). Increasing the enzyme concentration 2-fold also yielded near superimposition of the 2AP and RHX signals but with increased rate constants. Clear in the 2AP data is a small (∼15%) amplitude component with a slower (0.55 s^{-1}) effective rate constant (Figure 3) that is independent of M.*Eco*RI concentration (data not shown).

The close synchrony of the two-color on-rate data (Figure 3) clearly shows that the disruption of base stacking occurs (nearly) simultaneously with DNA binding. However, direct comparison of the DNA binding and base-flipping data at the 50% extent of reaction point ($t = 37$ ms in Figure 3) reveals an approximately 4 ms lag between the normalized data sets. This lag can be analyzed as a unimolecular base unstacking transition which must occur at a rate of >195 s^{-1} after the DNA binding event (see below). These data disprove any models that propose M.*Eco*RI to undergo fast DNA binding followed by a slow base-flipping event.

Two-Color Observation of Protein Dissociation and Base Restacking. During the dissociation of M.*Eco*RI from target DNA, the extrahelical base must be reinserted into the DNA double helix. Analogous to the on-rate kinetic experiments described above, the temporal order of protein dissociation and base restacking has not previously been examined. Under catalytic conditions rapid methylation of the target base is followed by a slow release of the methylated DNA from M.*Eco*RI (*14*). Following catalysis, the restacking of the methylated target base may occur rapidly followed by a slow dissociation of M.*Eco*RI from the DNA. Alternatively, the restacking of the target base within the double helix may occur concertedly with, or following, the dissociation of the enzyme−DNA complex. Two-color off-rate data were

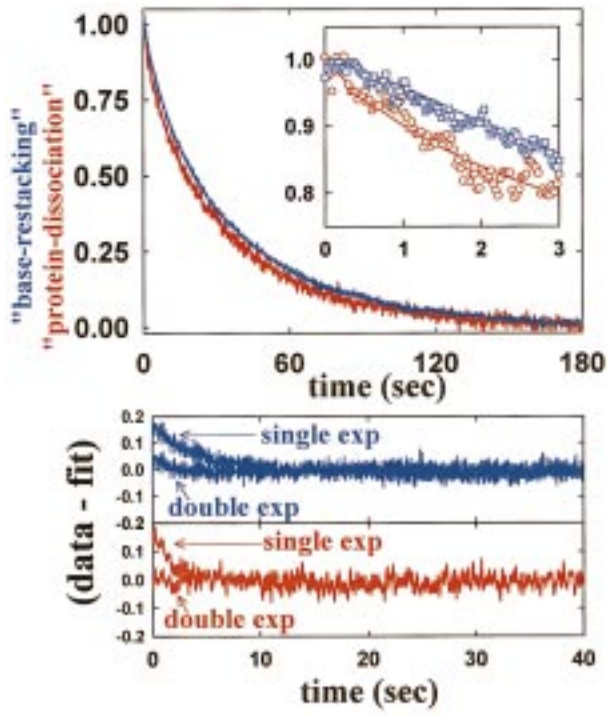

FIGURE 4: Determination of the absolute coupling between complex dissociation (red fluorescence signal) and target base restacking (blue fluorescence signal). Prebound ternary complexes (M.*Eco*RI−DNA−sinefungin) (200 nM) were rapidly mixed with the 100 μM 14 base pair DNA duplex lacking either modification in the stopped-flow system. The smooth lines represent the nonlinear least-squares fit to the data. Both data sets required double-exponential fits; 2AP base restacking data were best described using 0.72 exp(0.022t) + 0.28 exp(0.087t) and RHX complex dissociation data by 0.78 exp(0.026t) + 0.22 exp(0.178t). The inset shows data collected during the first 3 s of the off-rate time course. Note the ~0.5 s "lag" in the 2AP base restacking signal compared to the RHX dissociation signal. The residual plots for the single- and double-exponential fits are shown in the lower panel. The rate constants obtained from nonempirical analysis of these data directly in terms of the coupling between complex dissociation and base restacking are shown in Scheme 1 and described in the text.

obtained to specifically investigate these different mechanisms. The restoration of nearest-neighbor base-stacking interactions was examined by the quenching of the 2AP fluorescence intensity while the dissociation of the complex was followed by the decrease in the RHX fluorescence anisotropy signal. The approach to equilibrium was measured by a competition assay with stopped-flow data obtained following the rapid mixing of 200 nM ternary complex (M.*Eco*RI−DNA−sinefungin) with 100 μM 14 base pair duplex DNA lacking either modification (Figure 4).

Similar to the on-rate two-color experiments, protein dissociation and base restacking are (temporally) highly coupled processes. However, in contrast to the monophasic RHX binding signal changes observed during the on-rate experiments (Figures 2 and 3), the off-rate experiments revealed biphasic signal changes with nearly identical fractional amplitudes and rate constants. For the 2AP data, 28% of the amplitude was associated with a rate of 0.087 s^{-1} with the remaining 72% described by a rate of 0.022 s^{-1}. For the RHX data, 22% of the anisotropy signal decrease was associated with a rate of 0.178 s^{-1} and the remaining 78% slowly changing at 0.026 s^{-1}. *F*-statistical analysis confirms that double-exponential fits are superior to single-exponential fits for both signals at a 96% and >99% confidence level, respectively. The residuals for the single- and double-exponential fits to the off-rate data are shown in Figure 4 (lower panel).

Although the two-color off-rate data show that base restacking and complex dissociation are highly coordinated processes, it is clear that base restacking does not occur prior to complex dissociation. In fact, the restacking of the target base is reproducibly slower than the dissociation of the complex (Figure 4 inset). At the 50% point in the extent of the reaction graph in Figure 4 (t = 18.57 s), a net lag of 2.3 s occurs between the RHX and 2AP signals. Almost all of this lag (between complex dissociation and base restacking) occurs during the first 0.5 s of the experiment and is associated with a very slow base restacking rate for the fast-dissociating species. Because the two rate processes are so well resolved, the magnitude and duration of distortion in the residual plots for single-exponential fits (Figure 4, lower panel) yield an indicator of the amplitude (note ~20% distortion) and rate constant (distortion over within 2−5 s) of the missing fast component.

A Model for Enzyme−DNA Interaction. The two-color on-rate experiments clearly reveal that the binding of the DNA and the distortion of the target base away from B-form are kinetically linked. DNA binding occurs with a second-order association rate constant of 1.7 × 10^7 M^{-1} s^{-1} (Figure 2) and is in near synchrony with the unstacking of the target base (Figure 3). However, the DNA binding and base-flipping data superimpose only during the dominant (~80%) fast phase of the 2AP time course. The 2AP base-flipping signal has an additional component (~20%) with an enzyme concentration-independent effective rate of 0.55 s^{-1} that is not apparent in the RHX binding data. The concentration independence of this phase (increase of 2AP quantum yield) and lack of a similar slow phase in the RHX anisotropy signal strongly indicate that it represents an enzyme−DNA isomerization reaction involving the target base. The binding signal is invariant during this slow increase in 2AP fluorescence intensity because there is no significant change in the rotational motion of the DNA as it is already saturated with bound M.*Eco*RI.

The off-rate data are clearly double exponential in both RHX and 2AP signals (Figure 4). Because the RHX binding signal is monophasic during complex formation and biphasic during complex dissociation, the simplest interpretation of these data is that the isomerization step in the on-rate experiments (Figure 3) generates an enzyme-bound DNA species with a distinct off-rate. The measured off-rates are 0.024 and 0.18 s^{-1}, but from these data in isolation it is not possible to assign specific off-rates to the discrete enzyme−DNA configurations. However, the relative fractional amplitudes are helpful in this regard. The amplitudes of both the RHX and 2AP off-rate signal changes are about 20% fast and 80% slow and essentially match the 80% fast and 20% slow amplitudes observed during the 2AP on-rate experiment. Similarly, the amplitude of the slow 2AP phase matches the amplitude of both the fast 2AP and RHX off-rate phases. Hence, in this manner, it appears that the slowest off-rate is associated with the fastest forming enzyme−DNA species.

The above logic was directly implemented in a general purpose global nonlinear leasts-squares program (*23*, Globals Unlimited, Urbana, IL), enabling the simultaneous analysis

Scheme 1: Model for the M.*Eco*RI Interaction with Two-Color DNA[a]

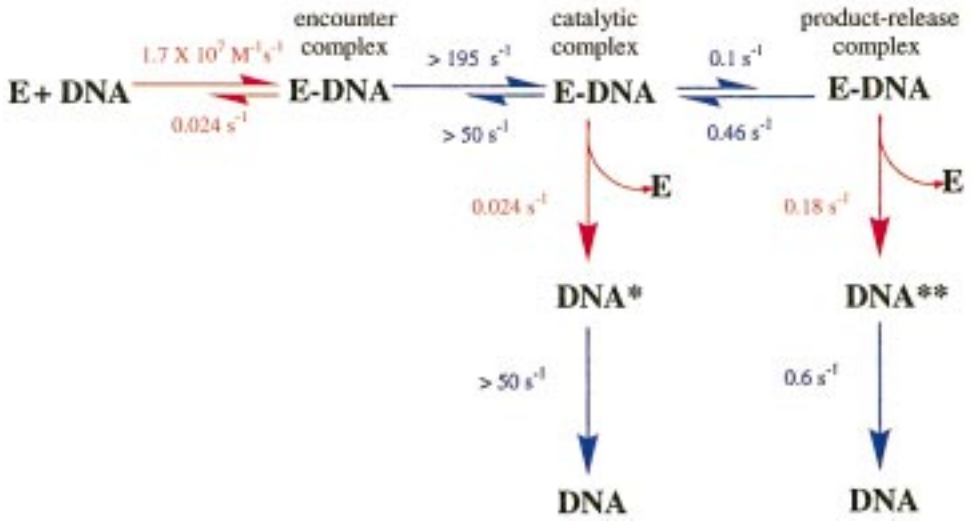

[a] Global simultaneous analysis of both the on-rate data and off-rate data from the rhodamine-x assay and 2-aminopurine base-stacking assay was performed in terms of the finite difference solution of this kinetic model. Rate constants uniquely linked to the anisotropy assay and 2AP assay are color-coded red and blue, respectively. The initially bound encounter complex undergoes a very rapid base-flipping reaction, with a rate >195 s^{-1} (~4 ms delay between binding and flipping). This "catalytic complex" isomerizes to a product-release state, with an enhanced off-rate for DNA. The flipped base restacks into B-DNA with a much slower rate from the product-release complex (0.6 s^{-1}) than from the catalytic complex (>50 s^{-1}) (see text for further details). Error estimations: 1.1×10^7 M^{-1} $s^{-1} \leq k_{on} \leq 2.25 \times 10^7$ M^{-1} s^{-1}, off-rates ±15%, and isomerization rates ±35%.

of all of the two-color on-rate and off-rate data in terms of an internally consistent kinetic mechanism. The clear advantage of this type of analysis is that it allows the rigorous combination of all the different data types in terms of an internally consistent kinetic model. For instance, information from the amplitude terms of both off-rate analyses is directly coupled to the fitting of the fundamental isomerization on-rate constants. Similarly, the small lag between the DNA binding and base-flipping signals, as well as the complex dissociation and base-restacking signals, can be analyzed directly for the first-order transitions linking these processes. In this manner, a single nonlinear analysis of the concentration-dependent on-rate and off-rate two-color experiments was performed (40 000 data points, eight separate experiments). The numerical values for all of the rate processes are shown in Scheme 1.

The constrained global analysis fits were able to represent the data as well as the empirical sums-of-exponential models applied to the individual data sets. The ratio of the global-fit χ^2 to the empirical-fit χ^2 value is 1.03 (perfect global-fit ratio would be 1.0), indicating that rigorous implementation of Scheme 1 was an adequate representation of all of the data. Note that the linking of the population terms between the on-rate and off-rate experiments allowed the deconvolution of the 0.55 s^{-1} effective rate (with contributions from both the "forward" and "reverse" isomerization steps) into two fundamental rate processes of 0.1 and 0.46 s^{-1} (Scheme 1). In addition, as expected from the near synchrony of the DNA binding and base-flipping events (Figure 3), the global analysis revealed that base flipping must occur at a rate greater than ~195 s^{-1} after binding to generate RHX anisotropy traces and 2AP fluorescence enhancements that are this closely coupled.

The kinetic coupling between enzyme−DNA complex dissociation and target base restacking is also temporally tightly linked; however, a distinct lag is evident in the off-rate data (Figure 4). Essentially all of the time lag between complex dissociation and base restacking is associated with the 20% isomerized population generated in the slow phase of the on-rate experiment (see inset of Figure 4). As the fast-dissociating class of enzymes disengages the target DNA, the extrahelical 2AP base is left in a configuration that does not immediately reinsert into the DNA double helix. The rate constant for base restacking from this enzyme-bound state is extremely hindered and occurs at only 0.6 s^{-1} (± 20%). In contrast, base restacking associated with the slow-dissociating class of enzymes is much faster and occurs at a rate greater than 50 s^{-1}.

The combined analyses are consistent with the following kinetic mechanism for base flipping. As M.*Eco*RI approaches its target site from solution, it flips the target base out of the double helix in near synchrony with binding the DNA (~4 ms lag). Estimations of the methylation rate constant ($k_{methylation}$) measured by rapid quench-flow pre-steady-state burst kinetics (*7, 11*) closely correlate with the initial binding rate and base-flipping rate measured in this study. Consequently, DNA binding, base flipping, and the methylation of the target base must occur nearly simultaneously. This is certainly an unexpected result, in that it would be very easy to imagine a variety of rate-limiting conformational transitions that could isolate these three distinct processes. The TATA binding protein was also found to bind DNA, intercalate four phenylalanines, and bend the DNA in a single-step reaction (*30*). The fact that these (seemingly) rather difficult conformational transitions imposed on DNA can be performed in a single concerted step could be the result of highly efficient protein design or due to some unique property of DNA (conformational "plasticity") which is not yet well understood.

A slow isomerization reaction follows these initial DNA binding and base-flipping events that generates a distinct configuration of the target base. This isomerization is responsible for generating the divergence of the RHX and

2AP data observed during the slow phase of the on-rate experiments (Figure 3). The product-release state has an intrinsic off-rate for target DNA that is approximately 10-fold greater than the initially bound catalytic state. This off-rate represents the rate-limiting step associated with product formation by this enzyme. Steady-state measurements of k_{cat} recover a value of 0.12 s^{-1} (*14*), very consistent with the predicted rate-limiting off-rate of 0.18 s^{-1} (Scheme 1) obtained from this pre-steady-state study.

We also find that the target base in the product-release complex is stabilized in a dramatically altered configuration relative to the initially bound enzyme−DNA complex. This effect is reflected both in the increased relative quantum yield of 2AP and in the unique slow base-restacking kinetics associated with this enzyme−DNA species. The rate of base restacking associated with the product-release state is much slower (0.6 s^{-1}) than the rate of base restacking associated with the initially bound catalytic state (>50 s^{-1}) (see inset to Figure 4). If the flipped-base geometry were identical in both the catalytic and product-release states, one would have expected identical rate constants for restacking from each. The fact that the product-release state has a base restacking rate at least 80 times slower than the catalytic complex (0.6 vs >50 s^{-1}, Scheme 1) suggests a flipped-base bond rotation about an axis that is different than the original 180° rotation associated with the extrahelical base in the catalytic state. Enzyme dissociation and base restacking from the initially bound catalytic state occur essentially as the mirror image of the DNA binding (i.e., superimposing dissociation/restacking). This result further supports the fact that the initial DNA binding and base-flipping transitions do indeed occur in a nearly concerted manner. A recent ^{19}F-target base NMR study (*32*) has been able to resolve clear and distinct enzyme-bound forms of the flipped base in the cytosine 5-methyltransferase (M.*Hha*I), which may be very similar to the multiple states described in this study.

While the above interpretation of the two-color kinetics measured herein must remain rather speculative until the enzyme−DNA cocrystal structure of M.*Eco*RI is solved, it is obvious that this "multicolor" strategy enables the elucidation of mechanistic information which is very difficult (if not impossible) to obtain in any other manner. The crystal structure of the bound complex, of course, cannot reveal the temporal correlation between the binding and flipping event, which this study directly measures. The site-specific incorporation of multiple fluorescence probes within a single substrate (in this case DNA) allows a direct measurement of the coordination between distinct kinetic processes. The raw data reported here are clear and essentially model-independent. Any future mechanisms that might be proposed for the M.*Eco*RI−DNA−cofactor complex must be consistent with the very tight temporal correlations found in this work.

ACKNOWLEDGMENT

J.M.B. acknowledges Prof. Myron F. Goodman (University of Southern California) for initially suggesting the use of 2-aminopurine to study DNA polymerases and Profs. James Lee (University of Texas Medical Branch, Galveston, TX) and C. Royer (INSERM, France) for pioneering work using fluorescence anisotropy to study protein−DNA interactions.

REFERENCES

1. Klimasauskas, S., Kumar, S., Roberts, R. J., and Cheng, X. (1994) *Cell 76,* 357−369.
2. Reinisch, K. M., Chen, L., Verdine, G. L., and Lipscomb, W. N. (1995) *Cell 82,* 143−153.
3. Labahn, J., Granzin, J., Schluckebier, G., Robinson, D. P., Jack, W. E., Schildkraut, I., and Sanger, W. (1994) *Proc. Natl. Acad. Sci. U.S.A. 91,* 10957−10961.
4. Gong, W., O'Gara, M., Blumenthal, R. M., and Cheng, X. (1997) *Nucleic Acids Res. 25,* 2702−2715.
5. Allan, B. W., and Reich, N. O. (1996) *Biochemistry 35,* 14757−14762.
6. Cal, S., and Connolly, B. A. (1996) *J. Biol. Chem. 271,* 1008−1015.
7. Allan, B. W., Beechem, J. M., Lindstrom, W., and Reich, N. O. (1998) *J. Biol. Chem. 273,* 2368−2373.
8. Malone, T., Blumenthal, R. M., and Cheng, X. (1995) *J. Mol. Biol. 253,* 618−632.
9. Vassylyev, D. G., Kashiwagi, T., Mikami, Y., Ariyoshi, M., Iwai, S., Ohtsuka, E., and Morikawa, K. (1995) *Cell 83,* 773−782.
10. Slupphaug, G., Mol, C. D., Kavli, B., Arvai, A. S., Krokan, H. E., and Tainer, J. A. (1996) *Nature 384,* 87−92.
11. Reich, N. O., and Mashhoon, N. (1993) *J. Biol. Chem. 268,* 9191−9193.
12. Greene, P. J., Heyneker, H. L., Bolivar, F., Rodriquez, R. L., Betlach, M. C., Covarrubias, A. A., Backman, K., Russel, D. J., Tait, R., and Boyer, H. W. (1978) *Nucleic Acids Res. 5,* 2373−2380.
13. Rubin, R. A., and Modrich, P. (1977) *J. Biol. Chem. 252,* 7265−7272.
14. Reich, N. O., and Mashoon, N. (1991) *Biochemistry 30,* 2933−2939.
15. Perez-Howard, G. M., Weil, P. A., and Beechem, J. M. (1995) *Biochemistry 34,* 8005−8017.
16. Fasman, G. D., Ed. (1975) *Handbook of Biochemistry and Molecular Biology,* 3rd ed., Vol. II, p 589, CRC Press, Cleveland, OH.
17. Ward, D. C., Reich, E., and Stryer, L. (1969) *J. Biol. Chem. 244,* 1228−1237.
18. Bloom, L. B., Otto, M. R., Beechem, J. M., and Goodman M. F. (1993) *Biochemistry 32,* 11247−11258.
19. Heyduk, T., and Lee, J. C. (1990) *Proc. Natl. Acad. Sci. U.S.A. 87,* 1744−1748.
20. LeTilly, V., and Royer, C. A. (1993) *Biochemistry 32,* 7753−7758.
21. Dunkak, K. S., Otto, M. R., and Beechem, J. M. (1996) *Anal. Biochem. 243,* 234−244.
22. Bloom, L. B., Turner, J., Kelman, Z., Beechem, J. M., O'Donnell, M., and Goodman, M. F (1996) *J. Biol. Chem. 271,* 30699−30708.
23. Beechem, J. M. (1992) *Methods Enzymol. 210,* 37−53.
24. Surby, M. A., and Reich, N. O. (1996) *Biochemistry 35,* 2209−2217.
25. Surby, M. A., and Reich, N. O. (1996) *Biochemistry 35,* 2201−2208.
26. McCammon, A. J., and Northrup, S. C. (1981) *Nature 293,* 316−317.
27. Schmitz, K. S., and Schurr, J. M. (1972) *J. Phys. Chem. 76,* 534−545.
28. Reich, N. O., and Mashhoon, N. (1990) *J. Biol. Chem. 265,* 8966−8970.
29. Reich, N. O., Maegley, K. A., Shoemaker, D. D., and Everett, E. (1991) *Biochemistry 30,* 2940−2946.
30. Parkhurst, K. M., Brenowitz, M., and Parkhurst, L. J. (1996) *Biochemistry 35,* 7459−7469.
31. McCullough, A. K., Dodson, M. L., Scharer, O. D., and Lloyd, R. S. (1997) *J. Biol. Chem. 272,* 27210−27217.
32. Klimasauskas, S., Szyperski, T., Serva, S., and Wüthrich, K. (1998) *EMBO J. 17,* 317−324.

BI9900020